Journal of Applied Phycology (2020) 32:3295–3304
https://doi.org/10.1007/s10811-020-02174-5

Transcriptomic exploration of genes related to the formation of archeospores in *Pyropia yezoensis* (Rhodophyta)

Shanshan Song [1,2,3] · Dahai Gao [1,2,3] · Xinghong Yan [1,2,3]

Received: 28 March 2020 / Revised and accepted: 1 June 2020 / Published online: 26 June 2020

Abstract

As an economically important marine seaweed, *Pyropia yezoensis* can be asexually reproduced via archeospores. However, the molecular mechanism of archeospore formation remains unclear. In this study, we characterized the transcriptomes of two strains of *Py. yezoensis*, which are strain *W′* with abundant archeospores and strain *W* with scarce archeospores. The 25- and 35-day-old gametophytic blades of both strains were sampled for RNA sequencing. Based on comparative transcriptomic analysis, a large number of differential expressed genes (DEGs) of four pairwise groups between samples were generated. In an effort to identify the genes related to archeospore formation, 415 consensus DEGs reflecting the difference between two strains were investigated. Gene ontology and KEGG analysis revealed that the function for these DEGs was enriched in various processes, such as translation, ribosome assembly, RNA methylation, vesicles assembly, intracellular localization of organelles, and endocytosis. According to functional analysis on 80 selected DEGs, it indicated that genes involved in calcium and MAPK signaling pathway, cytoskeletal movement, and cell wall degradation were related to the formation of archeospores. The accuracy of RNA-seq results was validated by quantitative real-time PCR of 8 selected DEGs. These findings suggest that the molecular mechanism of archeospore formation in *Py. yezoensis* is sophisticated and our results will serve as an essential foundation for further studies.

Keywords *Pyropia yezoensis* · Bangiales · Archeospores · Transcriptome · DEG · Signaling pathway

Introduction

The red marine alga *Pyropia yezoensis* is one of the economically important maricultural crops, (Sutherland et al. 2011). This alga has been extensively cultivated in Japan, China, and Korea and has the highest commercial value per unit mass in comparison with other algal cultivars (Kim et al. 2017).

Electronic supplementary material The online version of this article (https://doi.org/10.1007/s10811-020-02174-5) contains supplementary material, which is available to authorized users.

✉ Xinghong Yan
xhyan@shou.edu.cn

[1] Key Laboratory of Exploration and Utilization of Aquatic Genetic Resources, Ministry of Education, Shanghai Ocean University, 999 Huchenghuan Road, Lingang New City, Shanghai 201306, China

[2] National Demonstration Center for Experimental Fisheries Science Education, Shanghai Ocean University, 999 Huchenghuan Road, Lingang New City, Shanghai 201306, China

[3] Shanghai Engineering Research Center of Aquaculture, Shanghai Ocean University, 999 Huchenghuan Road, Lingang New City, Shanghai 201306, China

Pyropia yezoensis presents several interesting evolutionary, physiological, and ecological characteristics related to its development and reproduction. The life cycle of *Py. yezoensis* consists of alternation between two heteromorphic stages, the diploid filamentous sporophyte stage and the haploid foliose gametophyte stage. The reproductive ways of *Py. yezoensis* have been revealed to be versatile. In addition to the classic sexual reproduction, it exhibits asexual reproduction through the production of archeospores from young gametophytic blades (Shimizu et al. 2007; Mikami et al. 2019). Archeospore formation has been observed in several *Pyropia* species, such as *Py. tenera*, *Py. suborbiculata*, and *Py. chauhanii* (Tseng and Chang 1954; Song and Yan 2015; Yang et al. 2019).

During the process of archeospore formation the color and shape of differentiated vegetative cells of the gametophytic blade change, and then, a single spore is released and germinates into another gametophytic blade (Ma and Shen 1996). Archeospore formation is an important feature of great economic value, which has been explored to develop new techniques and patterns for germling production. In field cultivation archeospores provide a large number of secondary germlings and increase the yield on the cultivating net (Li

1984; Yan et al. 2004). Furthermore, the characteristics of archeospore germlings excel those of conchospore germlings in terms of growth speed and stress tolerance abilities (Li 1984). Nevertheless, there are trade-offs between archeospore formation and blade growth, as too many archeospores will slow the growth of blades. Therefore, a thorough understanding of this biological trait is needed ahead of application.

It has been shown that the formation and release of archeospores can be affected by several culture conditions, including light intensity, photoperiod, water temperature, salinity, and desiccation (Li and Wang 1987, 1984; Li et al. 1988, 1986; Kitade et al. 2008; Xu et al. 2019). Moreover, the production of archeospores is significantly accelerated by the exogenous addition of allantoin and ammonium sulfate (Li and Wang 1987; Mizuta et al. 2003; Sun et al. 2018). Notably, it has been reported that chemical mutagenesis can generate stably inherited mutants with different archeospore-producing abilities (Yan et al. 2004; Zhang and Yan 2014), suggesting that archeospore formation is a genetically controlled trait of *Pyropia*. Recently, several studies were carried out to explore the physiological and molecular mechanisms for the formation and release of archeospores. For example, Gao et al. (2011) proposed that cell wall and photosynthetic properties were changed during archeospore formation in *Py. yezoensis*. It has also been found that photosynthesis-dependent Ca^{2+} influx triggered archeospore reproduction, and they also reported that oxidative stress could promote archeospore formation (Takahashi et al. 2010; Takahashi and Mikami 2017). However, the molecular mechanism of archeospore formation is still obscure as only a few preliminary studies have been carried out (Xu et al. 2003; Kitade et al. 2008; He et al. 2013).

In the present study, comparative transcriptomic analysis between abundant and scarce archeospores release strains of *Py. yezoensis* was conducted, and the genes related to archeospore formation were analyzed, providing valuable insights into the molecular basis of the archeospore formation in *Pyropia*.

Materials and methods

Algal materials and culturing conditions

Reliable materials for investigating archeospore characteristics require strains with different archeospore formation abilities and similar genetic backgrounds. To achieve this requirement, *Py. yezoensis* pure strains of *W′* and *W* were selected from the germplasm strains of our laboratory, with the former continuously producing archeospores and the latter scarcely forming archeospores. These strains were previously established by separating and purifying a spottedly variegated gametophytic blade, produced by progeny of the hybridization between red mutant (*fre-1*,♀) and wild type (*U-511*,♂) (Yan et al. 2000; Yan and Aruga 2000). Free-living conchocelis of the two strains were stored in the laboratory as described by Kato and Aruga (1984). The medium used for gametophytes was sterilized seawater containing MES medium (Wang et al. 1986), and the culture conditions were as follows: 19 ± 1 °C, 40 μmol photons m^{-2} s^{-1}, and 10 L: 14 D photoperiod.

Sampling settings and archeospore quantification

To determine the suitable sampling strategy for investigating the gene expression change during archeospore formation, the archeospore release abilities of the two strains were evaluated. For each strain, 500 individuals were randomly selected from 18-day-old (initialized from the germination of single conchospore) germlings, and the number of individuals releasing archeospores was recorded each day. The proportion of individuals releasing archeospores increased continuously in *W′* strain, while all individuals in *W* strain scarcely released archeospores (Fig. 1a). We sampled 25- and 35-day-old germlings of the two strains for transcriptomic sequencing, named *W′25d*, *W′35d*, *W25d*, and *W35d*, respectively. For each sample, 0.1–0.3 g of gametophytic blade was washed with distilled water and flash-frozen in liquid nitrogen before being stored in − 80 °C refrigerator.

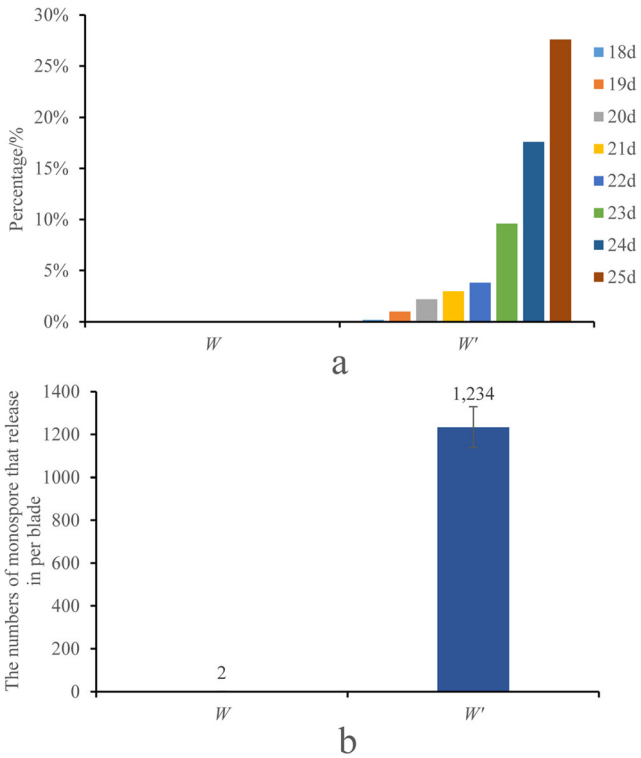

Fig. 1 Comparison of the ability of archeospore release between strain *W′* and *W*. **a** Percentage of individuals that release archeospores between strain *W′* and *W*. **b** Total numbers of archeospores per blade which been released from strain *W′* and *W*

Meanwhile, 10 individuals from 18-day-old germlings were employed to quantify the released archeospores of two strains. Plastic cups were used to cultivate the gametophytes, and the cups with new culture solution were replaced every day. The released archeospores were attached on the replaced cups, and they could grow into visible germlings after several days culturing. Next, the numbers of the archeospores germlings were counted by scraping them off from the cups, and the quantity of archeospores was equivalent to the overall amount of archeospores germlings. The total number of archeospores per blade was calculated for 7 days, and the experiment was repeated three times.

RNA extraction and sequencing

Total RNA from each algal sample was extracted using Trizol reagent (Thermo Fisher, USA). The absorbance at wavelengths of 260 nm and 280 nm (A_{260}/A_{280}) was measured by NanoDrop 2000, and the integrity was examined by 1% agarose gel electrophoresis and Agilent 2100. The RIN (RNA integrity number) value was confirmed to be greater than 6.0 for all samples, and 2 μg of total RNA was used as input material for sequencing library preparations. RNA sequencing was performed by the Illumina HiSeqXTen sequencing platform (NovelBio Bio-Pharm Technology Co. Ltd., Shanghai) following the standard library preparation procedures.

Transcriptome de novo assembly and annotation

Raw reads were quality filtered using Fast-QC (http://www.bioinformatics.babraham.ac.uk/projects/fastqc/), and the clean data were used for the downstream analyses. De novo assembly of a reference transcriptome from the pair-ended reads was carried out using Trinity (Haas et al. 2013), and putative open reading frames were predicted with OrfPredictor (Min et al. 2005). Clean RNA-seq reads were mapped to the reference transcriptome assembly with BWA-MEM (Li and Durbin 2009), and expression levels of the transcripts were quantified as fragments per kilobase of exon per million fragments mapped (FPKM).

Differential expression analysis

Differential expression analysis was conducted for four comparisons combined by four samples (*W′25d*, *W′35d*, *W25d*, and *W35d*), which were *W35d* vs *W25d*, *W′35d* vs *W′25d*, *W′25d* vs *W25d*, and *W′35d* vs *W35d*. The R package of EBseq was used to identify the differential expression genes (DEGs) with setting the criteria for differential screening at *P* value < 0.05, FDR ≤ 0.05, and $\log_2^{|FC|} \geq 1$.

Gene ontology and KEGG enrichment analysis of DEGs

GO enrichment analysis for DEGs was performed using the GOseq R package (Young et al. 2010). The GO terms with corrected *P* values under 0.05 were defined as significantly enriched terms for DEGs. In addition, KEGG annotations were performed based on the KEGG database (http://www.genome.jp/kegg/pathway.html), and pathways with corrected *P* values under 0.05 were defined as significantly enriched pathways for DEGs.

Expressional validation of DEGs with qRT-PCR

For qRT-PCR validation, eight genes representing different expression patterns were selected from DEGs. The primers were designed in the open reading frame region using NCBI Primer Blast (Table 1). RNA of each sample was reversely transcribed into cDNA using Takara reverse transcription kit (Takara, Japan). qRT-PCR was performed with Takara's SYBR Green fluorescent dye and Bio-Rad CFX-96 real-time PCR system using cDNA as a template and *18S* as an internal reference gene. Three biological replicates were set for each gene, and three technical replicates were set for each biological replicate. The relative expression level of each gene was calculated by the $2^{-\Delta\Delta Ct}$ method.

Availability of data and materials

All RNA sequencing data were submitted to NCBI SRA database (https://www.ncbi.nlm.nih.gov/sra/) under study number SRP191712. The accession numbers of each are as follows: SRR8873477, SRR8873478, SRR8873475, and SRR8873476.

Results

Archeospore formation ability evaluation of two strains

To explore the molecular mechanism of archeospore reproduction, *W′* and *W* strains of *Py. yezoensis* were selected, and the archeospore formation ability was evaluated. For each strain, the proportions of releasing individuals were documented. When germlings cultured from 18- to 25-days-old, the blades of *W′* strain continuously formed archeospores, and nearly one third of the individuals began to release archeospores (Fig. 1a). However, the blades of *W′* strain hardly formed archeospores. Moreover, the amount of archeospores during 7 days cultivation was documented for two strains. In total, there were up to 1234 archeospores per blade in *W′* strain and only 2 in *W* strain (Fig. 1b), indicating that the ability of archeospore formation of *W′* strain was 617 times than that of *W* strain.

Table 1 Primers of qRT-PCR about DEGs during archeospore formation and release in *Py. yezoensis*

Gene ID	Primers	Primer sequences (5′-3′)	Annealing/ °C
Contig21827	F	CAGAAGAACACATTGCAGAA CGA	55.3
	R	GTGATGGTAAACCTGCAACGG	56.8
Contig15542	F	CAACCACTGGTCGTTGGTCT	57.8
	R	CGACCTTGCATTTTTGCAGC	55.8
DN39215	F	TACGCAATCTTCCTCGCGTT	56.8
	R	CACGTCGTAGAATACGCATGG	56.0
Contig13390	F	ACTCCTGGGGAGATGGTGATT	58.0
	R	ATGCATTGGCCCTGTATGGT	57.1
Contig11730	F	GAGAGGCGTTTGACCTATT	55.9
	R	CGTCCTTGTGTGGTTCA	54.2
Contig2228	F	AAGTTCTGGAGCGTCTTG	56.5
	R	TCCTTTCCCTCAATCGT	55.4
Contig16448	F	TGTCTGACCAACTCTCACA	56.5
	R	CAAGCATAAGCATTCTAAGG	56.0
Contig10141	F	CTTTGCCCAGTTCGTCC	57.3
	R	GATGTAACCGTCGCCGT	57.2
PH18S	F	GTCCAGAGCGCTTTGAGATG	59.8
	R	AACCCTAATTCCCCGTCACC	59.8

Sequencing and de novo assembly

Transcriptomic sequencing was performed by the Illumina HiSeqXTen sequencing platform, and approximately 39.5–55.2 million raw reads were produced for four sequencing libraries (Table 2). After filtering the low-quality reads, there were 46,327,654, 33,036,768, 39,605,176, and 34,710,324 clean reads for libraries of *W'25d*, *W'35d*, *W25d*, and *W35d*, respectively. Based on de novo assembly, a total of 53,689 contigs were obtained, and over 99% reads in four libraries could be mapped to these contigs.

Differential gene expression analysis

Differential expression analysis for pairwise comparison resulted in four groups (Fig. 2). In comparing of 35- to 25-day-old samples, distinct numbers of up- and downregulated differential expression genes (DEGs) were observed in the two strains. In *W′* strain, a total of 4705 (*W'35d* vs. *W'25d* group) DEGs were identified, the majority of which were upregulated DEGs. In *W* strain, 2365 DEGs (*W35d* vs. *W25d* group) were identified, and the numbers of up- and downregulated DEGs were similar. When comparing samples between different strains of the same age, the DEGs pattern was also distinct. For 25-day-old samples, the number of DEGs was 3031 (*W'25d* vs. *W25d* group), with more upregulated than downregulated ones. For 35-day-old samples, 635 DEGs (*W′*

Table 2 Assessment of transcriptome sequencing data quality and gene alignment rate in *Py. yezoensis*

Sample name	*W'25d*	*W'35d*	*W25d*	*W35d*
Raw reads	55,275,334	39,534,000	48,001,920	41,619,454
Clean reads	46,327,654	33,036,768	39,605,176	34,710,324
GC%	65.0	60.0	64.5	64.5
Total contig	53,689			
Mapped reads	46,168,793	32,836,296	39,443,646	34,629,042
Mapped rate/%	0.997	0.994	0.996	0.998

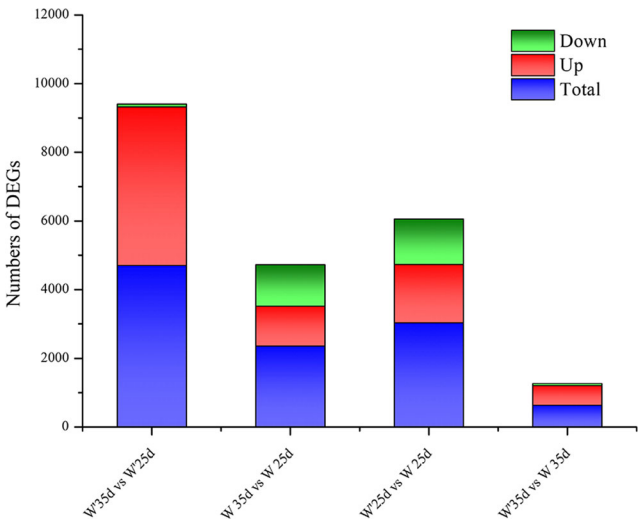

Fig. 2 Numbers of DEGs in different comparisons

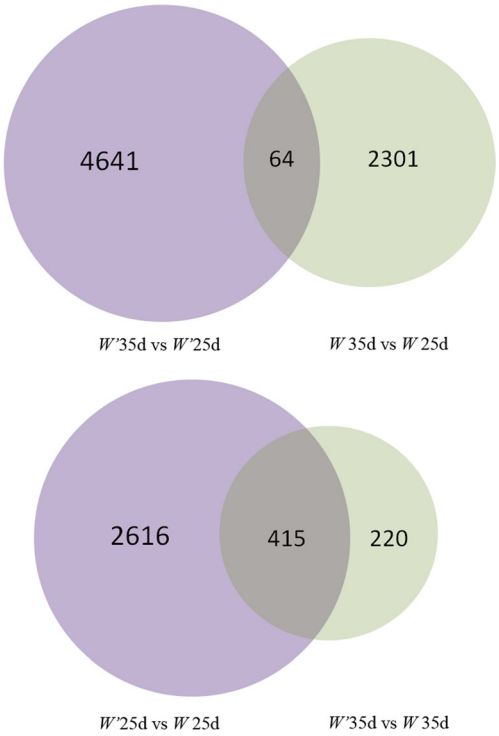

Fig. 3 Venn diagrams of DEGs. The sum of the numbers in the circle represents all of the DEGs produced in each comparison; the numbers in the overlapping parts represent the common DEGs between each comparison

35d vs. *W35d* group) were identified, the majority of which were upregulated ones.

In addition, consensus DEGs were identified between comparing groups (Fig. 3). According to Venn diagram illustration, the number of common DEGs between groups of *W'35d* vs. *W'25d* and *W35d* vs. *W25d* was only 64, and these common DEGs could account for the genes involved in normal developmental process. Likewise, there were 415 common DEGs between groups of *W'25d* vs. *W25d* and *W'35d* vs. *W35d*, which could be regarded as DEGs between the two strains at the same age. Among these 415 common DEGs, 361 were upregulated, and 54 were downregulated in *W'* strain, and the expression trends of each DEGs (up- or downregulation) in two comparing groups were identical (Table S2).

GO and pathway enrichment of common DEGs

As the 415 common DEGs were considered as genes reflecting the difference between two strains, the function of them might be related to the archeospore formation of *Py. yezoensis*. Gene ontology (GO) enrichment analysis showed that the functions were enriched in several basal biological processes, such as translation, RNA activity, actin and vesicle assembly, intracellular localization of Golgi and mitochondria, and peroxisome activity (Table S3). Among them, the GO terms of cytoplasmic translation, RNA methylation, and actin organization were highly enriched (Fig. 4).

Moreover, according to KEGG analysis, approximately 55% DEGs were mapped to 58 KEGG pathways (Table S4). The top significantly enriched pathways included ribosome assembly, endocytosis, carbon and nitrogen metabolism, photooxidation, as well as AGE-RAGE and MAPK signaling pathways (Fig. 5).

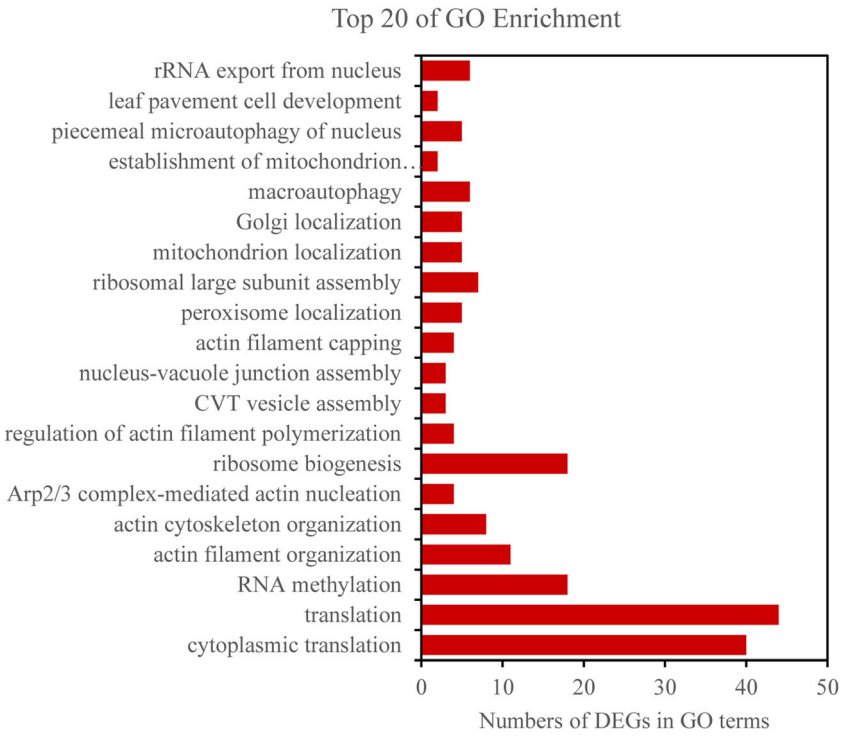

Fig. 4 GO enrichment of common DEGs between strain *W'* and *W*

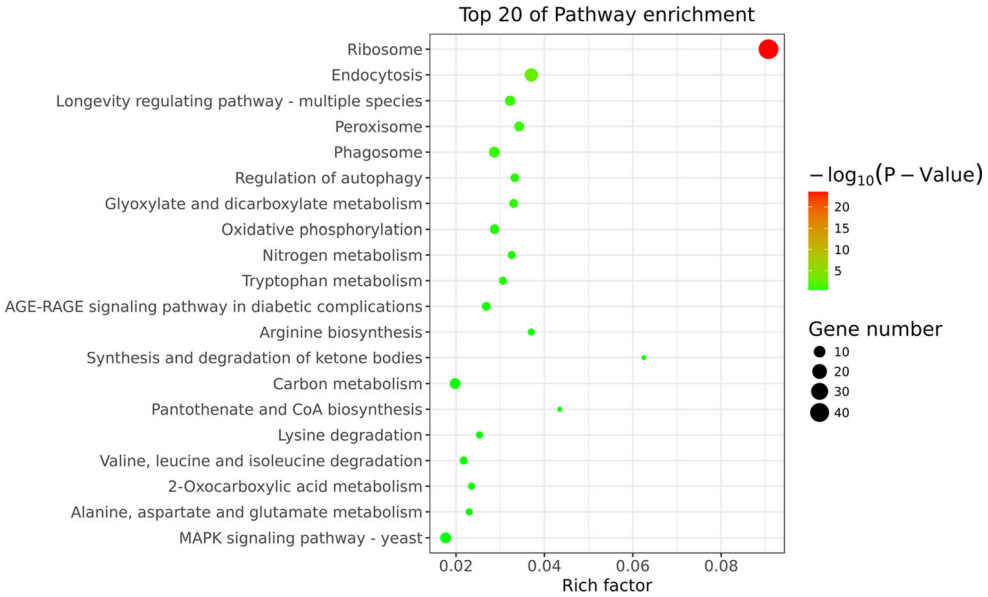

Fig. 5 KEGG enrichment of common DEGs between strain *W′* and *W*

Analysis of expression patterns of candidate DEGs

Based on consensus DEGs and functional enrichment screening, a total of 80 DEGs were further selected for hierarchical cluster analysis (Fig. 6). The result showed that the expression profiles of these genes were divergent between *W′* and *W* strain. Most DEGs were specifically upregulated in *W′* strain with abundant archeospores, suggesting that these genes may play roles in the process of archeospore formation. In terms of functional annotation, the constitution of these DEGs was as follows: 3 dehydrogenase genes and 17 Rab small GTPase genes, 6 myosin and 11 actin genes, 13 calmodulin (CaM) genes and 5 MAPKK kinase genes, 21 E3 ubiquitin ligase-related genes, 3 chitinase genes, and one gene encoded extracellular matrix protein.

qRT-PCR validation of candidate DEGs

To confirm the RNA-seq results, the expression levels of eight genes were quantified via qRT-PCR, and the expression levels (FPKM) among four samples were compared. The results showed that the expression patterns for all detected genes via qRT-PCR were consistent with RNA-Seq results, suggesting the reliability of transcriptomic data (Fig. 7).

Discussion

DEGs analysis revealed archeospore formation-related genes

The archeospore formation of *Py. yezoensis* was initialized by specialization of vegetative cells, and these specific cells could release archeospores which eventually germinated into gametophytic blades (Nelson et al. 1999). However, the molecular mechanisms underlying such asexual reproductive process remain unclear. In the present study, as the archeospore formation abilities of *W′* strain were 617 times than that of *W* (Fig. 1b), we deduced that such trait difference could be determined by distinct regulatory mechanism of two strains. By comparative transcriptomic analysis, the dynamic changes of gene expression were investigated. Notably, the 415 common DEGs between two strains could be defined as genes related to archeospore formation, in which 80 DEGs were further selected according to functional screening. Here, we focused on the genes with the function of cellular signaling pathways, cytoskeletal movement, and cell wall degradation, representing three regulatory processes during archeospore formation.

Annotation analysis of cellular signaling pathways

The Ca^{2+} signaling pathway mainly relies on Ca^{2+}/calmodulin (CaM) and calcineurin to initiate intracellular responses and participate in a variety of biological processes in eukaryotes (Clapham 2007). As the key component of Ca^{2+} signaling pathway, CaM mediates diverse biological processes, such as cell differentiation, cell movement, cytoskeletal, and enzyme activity regulation (Berridge et al. 2003). It has been reported that extracellular Ca^{2+} influx plays a critical role in the production of archeospores from *Py. yezoensis* (Li et al. 2009; Takahashi et al. 2010). Moreover, mitogen-activated protein kinase (MAPK) cascades were the evolutionary conserved signaling modules in all eukaryotes, playing key roles

Fig. 6 Heat map showing the expression profiles of selected DEGs in four samples. Hierarchical clustering was performed with gene expression values using the program TBtools

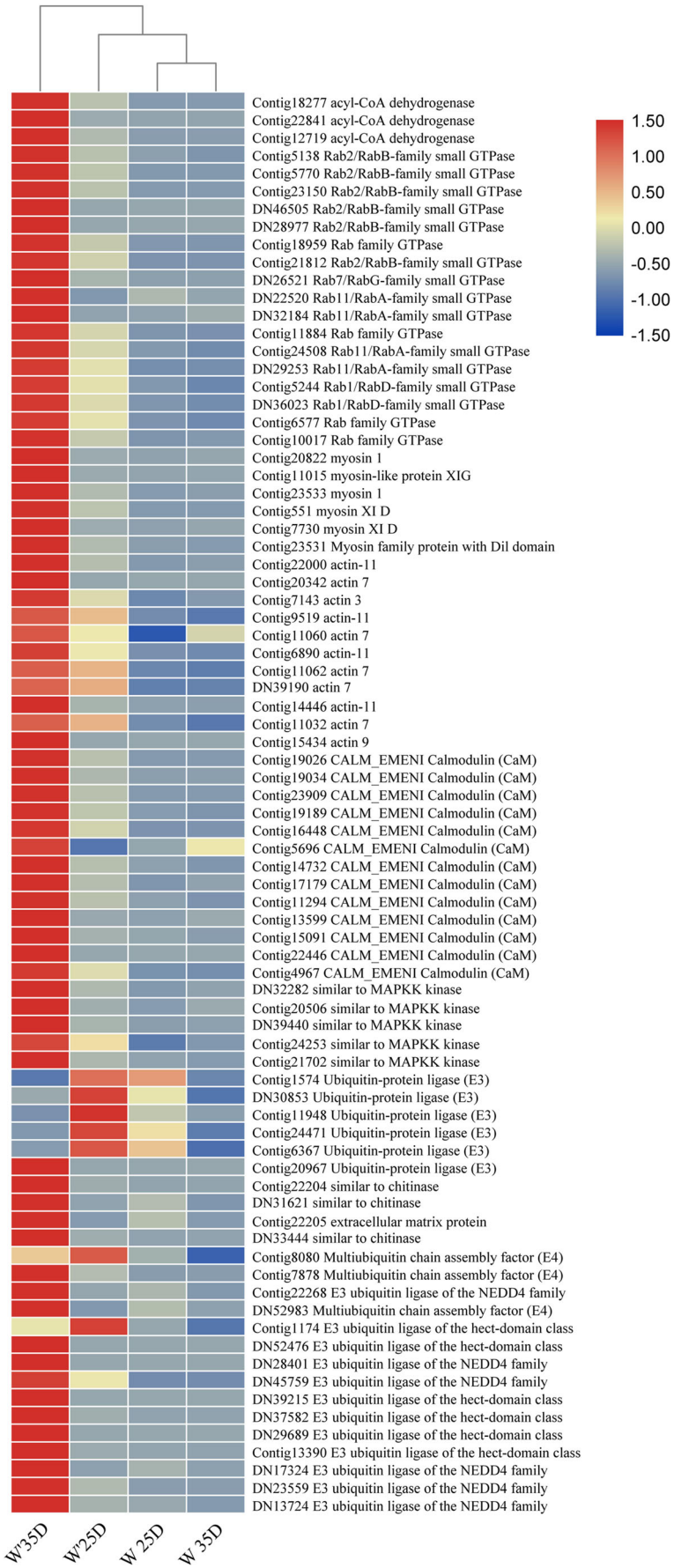
Contig18277 acyl-CoA dehydrogenase
Contig22841 acyl-CoA dehydrogenase
Contig12719 acyl-CoA dehydrogenase
Contig5138 Rab2/RabB-family small GTPase
Contig5770 Rab2/RabB-family small GTPase
Contig23150 Rab2/RabB-family small GTPase
DN46505 Rab2/RabB-family small GTPase
DN28977 Rab2/RabB-family small GTPase
Contig18959 Rab family GTPase
Contig21812 Rab2/RabB-family small GTPase
DN26521 Rab7/RabG-family small GTPase
DN22520 Rab11/RabA-family small GTPase
DN32184 Rab11/RabA-family small GTPase
Contig11884 Rab family GTPase
Contig24508 Rab11/RabA-family small GTPase
DN29253 Rab11/RabA-family small GTPase
Contig5244 Rab1/RabD-family small GTPase
DN36023 Rab1/RabD-family small GTPase
Contig6577 Rab family GTPase
Contig10017 Rab family GTPase
Contig20822 myosin 1
Contig11015 myosin-like protein XIG
Contig23533 myosin 1
Contig551 myosin XI D
Contig7730 myosin XI D
Contig23531 Myosin family protein with Dil domain
Contig22000 actin-11
Contig20342 actin 7
Contig7143 actin 3
Contig9519 actin-11
Contig11060 actin 7
Contig6890 actin-11
Contig11062 actin 7
DN39190 actin 7
Contig14446 actin-11
Contig11032 actin 7
Contig15434 actin 9
Contig19026 CALM_EMENI Calmodulin (CaM)
Contig19034 CALM_EMENI Calmodulin (CaM)
Contig23909 CALM_EMENI Calmodulin (CaM)
Contig19189 CALM_EMENI Calmodulin (CaM)
Contig16448 CALM_EMENI Calmodulin (CaM)
Contig5696 CALM_EMENI Calmodulin (CaM)
Contig14732 CALM_EMENI Calmodulin (CaM)
Contig17179 CALM_EMENI Calmodulin (CaM)
Contig11294 CALM_EMENI Calmodulin (CaM)
Contig13599 CALM_EMENI Calmodulin (CaM)
Contig15091 CALM_EMENI Calmodulin (CaM)
Contig22446 CALM_EMENI Calmodulin (CaM)
Contig4967 CALM_EMENI Calmodulin (CaM)
DN32282 similar to MAPKK kinase
Contig20506 similar to MAPKK kinase
DN39440 similar to MAPKK kinase
Contig24253 similar to MAPKK kinase
Contig21702 similar to MAPKK kinase
Contig1574 Ubiquitin-protein ligase (E3)
DN30853 Ubiquitin-protein ligase (E3)
Contig11948 Ubiquitin-protein ligase (E3)
Contig24471 Ubiquitin-protein ligase (E3)
Contig6367 Ubiquitin-protein ligase (E3)
Contig20967 Ubiquitin-protein ligase (E3)
Contig22204 similar to chitinase
DN31621 similar to chitinase
Contig22205 extracellular matrix protein
DN33444 similar to chitinase
Contig8080 Multiubiquitin chain assembly factor (E4)
Contig7878 Multiubiquitin chain assembly factor (E4)
Contig22268 E3 ubiquitin ligase of the NEDD4 family
DN52983 Multiubiquitin chain assembly factor (E4)
Contig1174 E3 ubiquitin ligase of the hect-domain class
DN52476 E3 ubiquitin ligase of the hect-domain class
DN28401 E3 ubiquitin ligase of the NEDD4 family
DN45759 E3 ubiquitin ligase of the NEDD4 family
DN39215 E3 ubiquitin ligase of the hect-domain class
DN37582 E3 ubiquitin ligase of the hect-domain class
DN29689 E3 ubiquitin ligase of the hect-domain class
Contig13390 E3 ubiquitin ligase of the hect-domain class
DN17324 E3 ubiquitin ligase of the NEDD4 family
DN23559 E3 ubiquitin ligase of the NEDD4 family
DN13724 E3 ubiquitin ligase of the NEDD4 family
1.50
1.00
0.50
0.00
-0.50
-1.00
-1.50
W'35D
W'25D
W 25D
W 35D

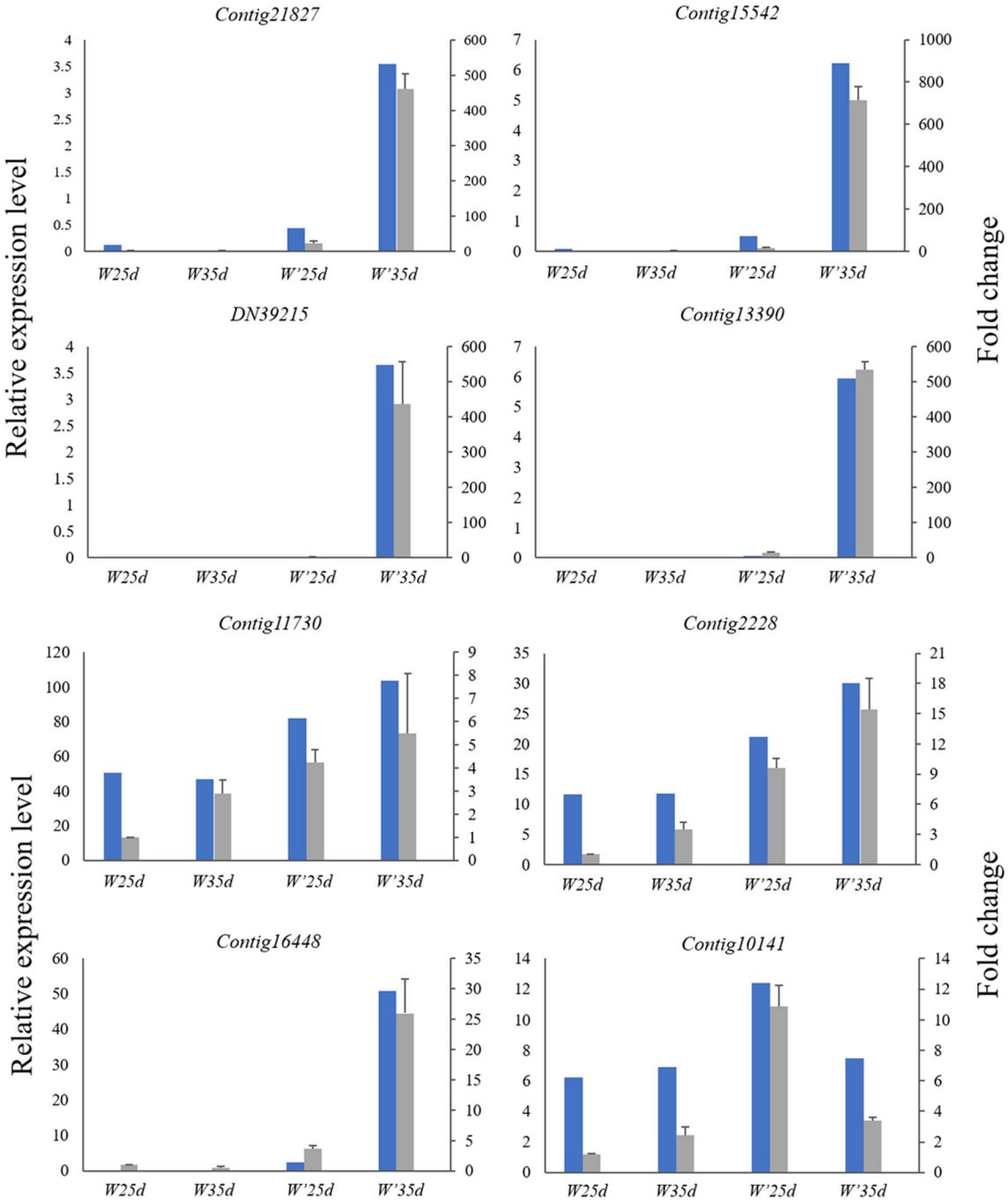

Fig. 7 Comparison of gene expression by RNA-seq and qRT-PCR. The y-axis on the left shows the expression data of RNA-seq (blue columns), while y-axis on the right shows corresponding relative gene expression levels ($2^{-\Delta\Delta Ct}$) analyzed by qRT-PCR (gray columns)

in gene expression and cytoplasmic activity. In yeast, the MAPK cascade regulates many spore formations and cell wall integration processes (Rodríguez-Peña et al. 2010). We found that 13 *CaM* and 5 MAPKK kinase homologous genes were highly expressed in *W'* strain (Fig. 6) and the MAPK signaling pathway was significantly enriched as the top 20 significant signaling KEGG pathways of the common DEGs (Fig. 5). Therefore, the regulatory roles of canalized signaling pathways as Ca^{2+} and MAPK are worthy of investigation.

Annotation analysis of cytoskeletal movement

The narrow cytoskeleton mainly referred as microfilaments, microtubules, and intermediate fibers, and the combination of actin and myosin can achieve cell movement in animals or cytoplasmic flow in plants. *Pyropia* species capable of dispersing archeospores can achieve cytoplasmic flow and cell morphological changes during the formation of archeospores. During the transformation of the vegetative cells into

archeospores, the shape of cell gradually became rounded by regular polygons and leads to the separation of protoplasts from the cell wall in the form of "water drop," leaving only a transparent gelatinous layer. Thus, it is possible that cytoskeletal movement is involved in such a process. We found that the expression of some actin and myosin homologous genes was upregulated in *W′* strain (Fig. 6), suggesting their roles in regulating the cytoskeletal changes of vegetative cells and causing the separation of protoplasts.

Annotation analysis of cell wall degradation

Enzymes isolated from marine animals and microorganisms, such as sea snail and *Pseudomonas*, can effectively hydrolyze the cell wall of algal vegetative cells (Han et al. 1997). The escape of archeospores from the constraint of the cell wall is required during the process of archeospore formation, although it was still unclear whether *Pyropia* can produce enzymes to digest the cell wall. In the present study, we found four chitinase homologous genes, and 17 Rab small GTPase genes were highly expressed in *W'35d* sample (Fig. 6). Chitinase belongs to the family of glycosyl hydrolases, which can effectively degrade the conidial wall of fungi (Adams 2004). As chitin is not the component of *Pyropia* cell wall, the role of these chitinases homologous in the degradation of *Py. yezoensis* cell wall is still debatable. On the other hand, the roles of Rab small GTPases in cell wall metabolism have been reported in land plants (Yang 2002; Lycett 2008), indicating that the potential function of these genes in archeospore formation should be investigated.

Conclusion

The comparative transcriptomic characteristics of *Py. yezoensis* strains were carried out for the first time. By exploring the DEGs between samples from two strains with different archeospore formation abilities, we suggest that the formation of archeospores was a complex regulatory process and multiple genes and pathways might be involved. The present study provides an important gene resource for deciphering the molecular mechanisms of archeospore formation, and further molecular, physiological, and phenotypic studies are required to better understand the asexual reproduction in *Pyropia*.

Acknowledgments The authors would like to thank Mr. Qingjie Zhang for technical assistance with experiments.

Funding information This study is supported in part by the National Key Research and Development Program of China (2018YFD0900606), National Natural Science Foundation of China (31072208), and Science and Technology Planning Project of Jiangsu Province, China (BE2018335).

Compliance with ethical standards

Competing interests The authors declare that they have no competing interests.

References

Adams DJ (2004) Fungal cell wall chitinases and glucanases. Microbiology 150:2029–2035

Berridge MJ, Bootman MD, Roderick HL (2003) Calcium signalling: dynamics, homeostasis and remodelling. Nat Rev Mol Cell Biol 4: 517–529

Clapham DE (2007) Calcium Signaling. Cell 131:1047–1058

Gao S, Wang GC, Yang RL, Xie XJ, Pan GH, Xu P, Zhu JY (2011) Variations in the cell walls and photosynthetic properties of *Porphyra yezoensis* (Bangiales, Rhodophyta) during archeospore formation. J Phycol 47:839–845

Haas BJ, Papanicolaou A, Yassour M, Grabherr M, Blood PD, Bowden J, Couger MB, Eccles D, Li B, Lieber M, MacManes MD, Ott M, Orvis J, Pochet N, Strozzi F, Weeks N, Westerman R, William T, Dewey CN, Henschel R, LeDuc RD, Friedman N, Regev A (2013) *De novo* transcript sequence reconstruction from RNA-seq using the trinity platform for reference generation and analysis. Nat Protoc 8: 1494–1512

Han BQ, Liu WS, Wang H, Dai JX (1997) Studies on the enzymes of algal cell wall hydrolysis. Mar Sci 21:47–49

He LW, Zhu JY, Lu QQ, Niu JF, Zhang BY, Lin AP, Wang GC (2013) Genetic similarity analysis within *Pyropia yezoensis* blades developed from both conchospores and blade archeospores using AFLP. J Phycol 49:517–522

Kato M, Aruga Y (1984) Comparative studies on the growth and photosynthesis of the pigmentation mutants of *Porphyra yezoensis* in laboratory culture. Jpn J Phycol 32:333–347

Kim JK, Yarish C, Hwang EK, Park M, Kim Y (2017) Seaweed aquaculture: cultivation technologies, challenges and its ecosystem services. Algae 32:1–13

Kitade Y, Asamizu E, Fukuda S, Nakajima M, Ootsuka S, Endo H, Tabata S, Saga N (2008) Identification of genes preferentially expressed during asexual sporulation in *Porphyra yezoensis* gametophytes (Bangiales, Rhodophyta). J Phycol 44:113–123

Li SY (1984) The ecological characteristics of monospores of *Porphyra yezoensis* Ueda and their use in cultivation. Hydrobiologia 116:255–258

Li H, Durbin R (2009) Fast and accurate short read alignment with burrows-wheeler transform. Bioinformatics 25:1754–1760

Li SY, Wang JC (1984) The influence of the light intensity on the formation, discharge and adherence of monospores. Mar Sci 8:41–43

Li SY, Wang JC (1987) The influence of the various concentrations of $(NH_4)_2SO_4$ on the growth of thalli of *Porphyra yezoensis* and the formation, discharge and adherence of monopores. Mar Sci 11:35–39

Li SY, Xu P, Wang M (1986) The influence of seawater on the discharge and adherence of monospores of *Porphyra yezoensis* Ueda. Mar Sci 10:38–40

Li SY, Xu P, Wang M (1988) Effect of light period on the growth of thalli and the formation, discharge and adherence of monospores of *Porphyra yezoensis* Ueda. Mar Sci 12:58–61

Li L, Saga N, Mikami K (2009) Ca^{2+} influx and phosphoinositide signalling are essential for the establishment and maintenance of cell polarity in monospores from the red alga *Porphyra yezoensis*. J Exp Bot 60:3477–3489

Lycett G (2008) The role of Rab GTPases in cell wall metabolism. J Exp Bot 59:4061–4074

Ma JH, Shin JA (1996) A study on monospores and leafy thalli of gametophytes of *Porphyra tenuipedalis*. J Fish China 20:132–138

Mikami K, Li CZ, Irie R, Hama Y (2019) A unique life cycle transition in the red seaweed *Pyropia yezoensis* depends on apospory. Commun Biol 2:299–308

Min XJ, Butler G, Storms R, Tsang A (2005) OrfPredictor: predicting protein-coding regions in EST-derived sequences. Nucleic Acids Res 33:W677–W680

Mizuta H, Yasui H, Saga N (2003) A simple method to mass produce monospores in the thallus of *Porphyra yezoensis* Ueda. J Appl Phycol 15:351–353

Nelson WA, Brodie J, Guiry MD (1999) Terminology used to describe reproduction and life history stages in the genus *Porphyra* (Bangiales, Rhodophyta). J Appl Phycol 11:407–410

Rodríguez Peña JM, García R, Nombela C, Arroyo J (2010) The high-osmolarity glycerol (HOG) and cell wall integrity (CWI) signalling pathways interplay: a yeast dialogue between MAPK routes. Yeast 27:495–502

Shimizu A, Morishima K, Kobayashi M, Kunimoto M, Nakayama I (2007) Identification of *Porphyra yezoensis* (Rhodophyta) meiosis by DNA quantification using confocal laser scanning microscopy. J Appl Phycol 20:83–88

Song JT, Yan XH (2015) Cytological studies on *Pyropia chauhanii* from Indian. J Fish China 39:1479–1486

Sun D, Ding HC, Yan XH (2018) The influence of allantoin on monospores release and somatic cell differentiation in gametophytic blades of *Pyropia chauhanii*. J Fish China 42:534–543

Sutherland JE, Lindstrom SC, Nelson WA, Brodie J, Lynch MDJ, Hwang MS, Choi HG, Miyata M, Kikuchi N, Oliveira MC, Farr T, Neefus C, Mols-Mortensen A, Milstein D, Mueller KM (2011) A new look at an ancient order: generic revision of the Bangiales (Rhodophyta). J Phycol 47:1131–1151

Takahashi M, Mikami K (2017) Oxidative stress promotes asexual reproduction and apogamy in the red seaweed *Pyropia yezoensis*. Front Plant Sci 8:62–67

Takahashi M, Saga N, Mikami K (2010) Photosynthesis–dependent extracellular Ca^{2+} influx triggers an asexual reproductive cycle in the marine red macroalga *Porphyra yezoensis*. Am J Plant Sci 1:1–11

Tseng CK, Chang TJ (1954) Studies on *Porphyra* I. Life history of *Pyropia tenera* Kjellm. Acta Bot Sin 3:287–302

Wang SJ, Zhang XP, Xu ZD, Sun YL (1986) A study on the cultivation of the vegetative cells and protoplasts of *P. haitanensis* I. Oceanol Limnol Sinica 17:217–221

Xu L, Zhou YH, Wang SJ, Wang YX, Ma LB, Zhou ZG (2003) Ultrastructural and molecular evidence for monospore formation in the thallus of *Porphyra yezoensis*. J Fish China 27:519–527

Xu D, Song XW, Li FT, Pan XH, Zhu WF, Zhang XC (2019) Effects of desiccation, diurnal temperature changes and irradiance on archeospore production of *Pyropia yezoensis*. Aquaculture 509: 167–170

Yan XH, Aruga Y (2000) Genetic analysis of artificial pigmentation mutants in *Porphyra yezoensis* Ueda (Bangiales, Rhodophyta). Phycol Res 48:177–187

Yan XH, Fujita Y, Aruga Y (2000) Induction and characterization of pigmentation mutants in *Porphyra yezoensis* (Bangiales, Rhodophyta). J Appl Phycol 12:69–81

Yan XH, Fujita Y, Aruga Y (2004) High monospore-producing mutants obtained by treatment with MNNG in *Porphyra yezoensis* Ueda (Bangiales, Rhodophyta). Hydrobiologia 512:133–140

Yang Z (2002) Small GTPases: versatile signaling switches in plants. Plant Cell 14:S375–S388

Yang XW, Ding HC, Yan XH (2019) Genetic analysis of the period of meiosis and morphogenesis of the gametophytic blades in *Pyropia suborbiculata* (Bangiales, Rhodophyta). J Appl Phycol 31:4061–4068

Young MD, Wakefield MJ, Smyth GK, Oshlack A (2010) Gene ontology analysis for RNA-seq: accounting for selection bias. Genome Biol 11:R14–R25

Zhang C, Yan XH (2014) Isolation and characterization of new strains of *Pyropia chauhanii* (Bangiales, Rhodophyta). J Fish China 38:1457–1465